AIAA JOURNAL
Vol. 42, No. 6, June 2004

Influence of Inflow Turbulence in Shock-Wave/Turbulent-Boundary-Layer Interaction Computations

G. A. Gerolymos,* E. Sauret,† and I. Vallet‡
Université Pierre-et-Marie-Curie, 75252 Paris, France

The influence of inflow turbulence on the results of Favre–Reynolds-averaged Navier–Stokes computations of supersonic oblique-shock-wave/turbulent-boundary-layer interactions (shock-wave Mach-number $M_{\mathrm{SW}} \sim 2.9$), using seven-equation Reynolds-stress model turbulence closures, is studied. The generation of inflow conditions (and the initialization of the flowfield) for mean flow, Reynolds stresses, and turbulence length scale, based on semi-analytic grid-independent boundary-layer profiles, is described in detail. Particular emphasis is given to freestream turbulence intensity and length scale. The influence of external-flow turbulence intensity is studied in detail both for flat-plate boundary-layer flow and for a compression-ramp interaction with large separation. It is concluded that the Reynolds-stress model correctly reproduces the effects of external flow turbulence.

Introduction

THE boundary-layer state at the beginning of the interaction with an oblique-shock wave has a major influence on the flowfield.[1,2] Various studies, both computational and experimental, have been published on the effects of Mach number M_∞, of Reynolds number based on boundary-layer thickness Re_{δ_0}, and of the boundary-layer kinematic shape factor H_{k_0} on the interaction.[1,2] On the other hand, the influence of freestream turbulence has not been extensively investigated, with the exception of the study by Raghunathan and McAdam[3,4] on the effects of turbulence intensity T_{u_∞} in transonic interactions (shock-wave Mach number $M_{\mathrm{SW}} = 1.44$), on a biconvex airfoil in a confined subsonic flow ($M_\infty = 0.68$–0.78). In 1985, these authors[4] stated in their introduction that "although there are several research reports on the effect of flow unsteadiness on boundary-layer transition and attached turbulent boundary-layers, there is scant information available as to the effect of flow unsteadiness in general and turbulence in particular on shock interactions." Despite the recent major advances in understanding the unsteadiness inherent in the interaction, the preceding statement is largely valid today.[2,5,6]

The purpose of the present paper is to study the influence of inflow freestream turbulence intensity T_{u_∞} and length scale ℓ_{T_∞} in oblique-shock-wave/turbulent-boundary-layer interactions. The investigation is based on the numerical integration of the Favre–Reynolds averaged Navier–Stokes equations with near-wall, wall-normal-free seven-equation Reynolds stress model (RSM) turbulence closures (see Refs. 7 and 8). The RSM closures, computational grids, and numerical procedure used are described in detail by Gerolymos et al.[9] Computations presented in this paper were carefully checked for grid convergence[9] and were systematically run with two different RSM closures: 1) the Gerolymos–Vallet[7] (GV RSM) and 2) a wall-normal, free version of the Launder–Shima geometric normals model [(WNF–LSS RSM) see Refs. 8 and 9]. Systematic assessment of these two RSM closures against experimental data for oblique-shock-wave/turbulent-boundary-layer interactions[9] has demonstrated the ability of these models to predict such flows, with the WNF–LSS[8,9] RSM slightly underpredicting separation and the GV[7] RSM slightly overpredicting separation.

Flowfield Initialization and Inflow Conditions

A review of relevant publications reveals that there are two ways for generating initial and inflow conditions for the computations: 1) to run a preliminary flat-plate zero-pressure-gradient boundary-layer computation[10] and 2) the use of semi-analytic boundary-layer profiles.[11] The second approach is of course simpler, provided all important inlet boundary-layer-profile features can be included with reasonable accuracy, that is, giving a satisfactory fit of the measured boundary-layer profile at the beginning of the interaction, which is of course situated farther downstream of the computational domain inflow. If the preliminary computations approach is chosen,[10] it is very difficult to match both the external flow turbulence and the correct boundary-layer integral parameters, that is, momentum thickness Reynolds number Re_{θ_0} and kinematic boundary-layer shape factor H_{k_0} at the beginning of the interaction, where $Re_{\theta_0} = \tilde{u}_e \theta_0 \breve{\nu}_e^{-1}$, $\tilde{u}_e$ is the mean-velocity at the boundary-layer edge,

$$\theta = \int_0^\delta \frac{\bar{\rho}\tilde{u}}{\bar{\rho}_e \tilde{u}_e}\left(1 - \frac{\tilde{u}}{\tilde{u}_e}\right) \mathrm{d}y$$

is the momentum thickness, $\breve{\nu}_e$ is the kinematic viscosity at the boundary-layer edge, $H_{k_0} = \delta^*_{k_0}\theta_{k_0}^{-1}$ is the kinematic boundary-layer shape factor,

$$\delta^*_k = \int_0^\delta \left(1 - \frac{\tilde{u}}{\tilde{u}_e}\right) \mathrm{d}y$$

is the kinematic displacement thickness,

$$\theta_k = \int_0^\delta \frac{\tilde{u}}{\tilde{u}_e}\left(1 - \frac{\tilde{u}}{\tilde{u}_e}\right) \mathrm{d}y$$

is the kinematic momentum thickness, and δ is the boundary-layer thickness, as well as the external-flow turbulence. The simple and versatile procedure described in the present paper is able to generate a boundary-layer profile for the mean velocity and for the turbulence variables (Reynolds stresses and turbulence length scale) and include arbitrary values for external flow turbulence (T_{u_e} and ℓ_{T_e}, where $T_{u_e} = \sqrt{(\frac{2}{3}k_e)}\tilde{u}_e^{-1}$ is the turbulence intensity at the boundary-layer edge and $\ell_{T_e} = k_e^{3/2}\varepsilon_e^{-1}$ is the turbulence length scale at the boundary-layer edge).

This procedure defines the vector of nonconservative variables describing the boundary-layer profile, in a local reference frame (x_{BL}, y_{BL}, z_{BL}), where x_{BL} is the tangent-to-the-wall direction,

Received 5 May 2003; presented as Paper 2003-3465 at the 33rd Fluid Dynamics Conference, Orlando, FL, 23–26 June 2003; revision received 4 November 2003; accepted for publication 13 November 2003. Copyright © 2004 by the authors. Published by the American Institute of Aeronautics and Astronautics, Inc., with permission. Copies of this paper may be made for personal or internal use, on condition that the copier pay the $10.00 per-copy fee to the Copyright Clearance Center, Inc., 222 Rosewood Drive, Danvers, MA 01923; include the code 0001-1452/04 $10.00 in correspondence with the CCC.

*Professor, Director, Laboratoire d'Energétique, Case 800, 4 place Jussieu; geg@ccr.jussieu.fr.

†Research Assistant, Laboratoire d'Energétique, Case 800, 4 place Jussieu; sauret@ccr.jussieu.fr.

‡Assistant Professor, Laboratoire d'Energétique, Case 800, 4 place Jussieu; vallet@ccr.jussieu.fr.

y_{BL} is the normal-to-the-wall coordinate, and z_{BL} is the normal to the $(x_{\text{BL}}, y_{\text{BL}})$ plane

$$\boldsymbol{v}_{\text{BL}} = \left[\bar{\rho}, \tilde{u}_{\text{BL}}, \tilde{T}, \widetilde{u''_{\text{BL}}u''_{\text{BL}}}, \widetilde{u''_{\text{BL}}v''_{\text{BL}}}, \widetilde{v''_{\text{BL}}v''_{\text{BL}}}, \widetilde{w''_{\text{BL}}w''_{\text{BL}}}, \varepsilon^*\right]^T$$
$$= \boldsymbol{v}_{\text{BL}}\left(y_{\text{BL}}/\delta; \tilde{u}_{\text{BL}_e}, \breve{p}_{t_e}, \breve{T}_{t_e}, \breve{M}_e, \tilde{T}_w, r_f, T_{u_e}, \ell_{T_e}, \delta\right) \tag{1}$$

where $\breve{p}_{t_e} = \bar{p}_e[1 + \frac{1}{2}(\gamma - 1)\breve{M}_e^2]^{\gamma/(\gamma-1)}$ is the total pressure at the boundary-layer edge, $\breve{T}_{t_e} = \tilde{T}_e + \tilde{u}_e^2/(2c_p)$ is the total temperature at the boundary-layer edge, $\tilde{u}_e$ and $\breve{M}_e = \tilde{u}_e/\sqrt{(\gamma R_g \tilde{T}_e)}$ are the velocity and the Mach number at the boundary-layer edge, respectively, $[u_{\text{BL}}, v_{\text{BL}}, w_{\text{BL}}]^T$ are the velocity components (parallel to the wall, perpendicular to the wall, and perpendicular to the plane), ε^* is the modified turbulent kinetic energy dissipation rate,[12] $\tilde{T}_w$ is the wall temperature, and r_f is the adiabatic-wall temperature-recovery factor. For all of the applications considered in the present work $r_f = 0.89$ was taken.[13] The procedure developed for computing $\boldsymbol{v}_{\text{BL}}$ [Eq. (1)] can be summarized as follows. For notational simplicity we drop the subscripts BL, with the assumption that in this section x is the tangent-to-the-wall direction, y is the normal-to-the-wall coordinate, and z is the normal-to-the (x, y) plane.

Compressibility Transformation

The Van Driest transformation[13] (also see Ref. 14), invoking the Morkovin hypothesis (see Ref. 15), is used to relate temperature and velocity profiles, and to define a corresponding incompressible flow $(\bar{u}_{e_{\text{inc}}})$,

$$\alpha_{\text{VD}}^2 = \frac{\tilde{T}_e}{\tilde{T}_w}\left(r_f \frac{\gamma - 1}{2}\breve{M}_e^2\right) = \frac{T_r - \tilde{T}_e}{\tilde{T}_w}, \qquad \beta_{\text{VD}} = \frac{T_r - \tilde{T}_w}{\tilde{T}_w}$$
$$\bar{u}_{e_{\text{inc}}} = \frac{\tilde{u}_e}{\alpha_{\text{VD}}}\left\{\arcsin\frac{2\alpha_{\text{VD}}^2 - \beta_{\text{VD}}}{\sqrt{4\alpha_{\text{VD}}^2 + \beta_{\text{VD}}^2}} + \arcsin\frac{\beta_{\text{VD}}}{\sqrt{4\alpha_{\text{VD}}^2 + \beta_{\text{VD}}^2}}\right\} \tag{2}$$

Incompressible Velocity Profile

The equivalent incompressible velocity profile is estimated using Spalding's velocity profile[16] $\bar{u}_{\text{S}}^+$ with an additional Coles[17] wake-parameter Π,

$$\bar{u}_{\text{inc}}^+ = \bar{u}_{\text{S}}^+ + \bar{u}_{\text{C}}^+, \qquad \bar{u}_{\text{C}}^+ = \frac{\Pi}{\kappa_{\text{VK}}}\left[1 - \cos\left(\frac{\pi y^+}{\delta^+}\right)\right]$$
$$y^+ = \bar{u}_{\text{S}}^+ + \mathrm{e}^{-\kappa_{\text{VK}}B}\left[\mathrm{e}^{\kappa_{\text{VK}}\bar{u}_{\text{S}}^+} - 1 - \kappa_{\text{VK}}\bar{u}_{\text{S}}^+ - \frac{\left(\kappa_{\text{VK}}\bar{u}_{\text{S}}^+\right)^2}{2!} - \frac{\left(\kappa_{\text{VK}}\bar{u}_{\text{S}}^+\right)^3}{3!}\right] \tag{3}$$

where the implicit definition of $\bar{u}_{\text{S}}^+$ [Eq. (3)] is solved by a Newton iteration procedure, $y^+ = (y\breve{u}_\tau)/\breve{\nu}_w$ is the nondimensional wall distance, $\bar{u}^+ = \bar{u}/\breve{u}_\tau$ is the nondimensional velocity expressed in wall units, $\breve{u}_\tau$ is the friction velocity, $\breve{\nu}_w$ is the cinematic viscosity at the solid wall, $\kappa_{\text{VK}} = 0.4$ is the von Kármán coefficient, and $B = 5.5$ (Ref. 16). It is straightforward (after some algebra) to compute analytically

$$\delta_{\text{inc}}^* = \int_0^\delta \left(1 - \frac{\bar{u}_{\text{inc}}}{\bar{u}_{e_{\text{inc}}}}\right)\mathrm{d}y, \qquad \frac{\mathrm{d}\bar{u}_{\text{inc}}}{\mathrm{d}y}$$

where $\mathrm{d}y^+/\mathrm{d}\bar{u}_{\text{S}}^+$ is computed by straightforward differentiation of Eq. (3):

$$\delta_{\text{inc}}^* = \delta - \frac{\breve{\nu}_w}{\bar{u}_{e_{\text{inc}}}}\left\{\frac{\left(\bar{u}_{e_{\text{inc}}}^+ - 2\Pi/\kappa_{\text{VK}}\right)^2}{2} + \exp\left(-\kappa_{\text{VK}}B\right)\right.$$
$$\times\left[\frac{1}{\kappa_{\text{VK}}}\exp\left[\kappa_{\text{VK}}\left(\bar{u}_{e_{\text{inc}}}^+ - \frac{2\Pi}{\kappa_{\text{VK}}}\right)\right]\right]\left\{\kappa_{\text{VK}}\left(\bar{u}_{e_{\text{inc}}}^+ - \frac{2\Pi}{\kappa_{\text{VK}}}\right) - 1\right\}$$
$$- \frac{\kappa_{\text{VK}}}{2}\left(\bar{u}_{e_{\text{inc}}}^+ - \frac{2\Pi}{\kappa_{\text{VK}}}\right)^2 - \frac{\kappa_{\text{VK}}^2}{3}\left(\bar{u}_{e_{\text{inc}}}^+ - \frac{2\Pi}{\kappa_{\text{VK}}}\right)^3 - \frac{\kappa_{\text{VK}}^3}{8}$$
$$\left.\times\left(\bar{u}_{e_{\text{inc}}}^+ - \frac{2\Pi}{\kappa_{\text{VK}}}\right)^4\right] + \exp(-\kappa_{\text{VK}}B)\frac{1}{\kappa_{\text{VK}}}\right\} - \frac{\Pi\delta}{\kappa_{\text{VK}}\bar{u}_{e_{\text{inc}}}^+} \tag{4}$$

$$\frac{\mathrm{d}\bar{u}_{\text{inc}}}{\mathrm{d}y} = \left(\frac{\mathrm{d}y^+}{\mathrm{d}\bar{u}_{\text{S}}^+}\right)^{-1}\frac{\breve{u}_\tau^2}{\breve{\nu}_w} + \frac{\breve{u}_\tau^2}{\breve{\nu}_w}\frac{\Pi\pi}{\kappa_{\text{VK}}\delta^+}\sin\left(\pi\frac{y^+}{\delta^+}\right) \tag{5}$$

Eddy Viscosity

The preceding velocity profile corresponds approximately to an eddy-viscosity distribution:

$$-\overline{u'v'} = \nu_{T_{\text{inc}}}\frac{\mathrm{d}\bar{u}_{\text{inc}}}{\mathrm{d}y}, \qquad \nu_{T_{\text{inc}}} = \nu_{T_{\text{out}}}\tanh\left(\frac{\nu_{T_{\text{in}}}}{\nu_{T_{\text{out}}}}\right) \tag{6}$$

with an inner eddy viscosity obtained from Spalding's law[16] and a Clauser[18] outer eddy viscosity:

$$\nu_{T_{\text{in}}} = \breve{\nu}_w\left(\frac{\mathrm{d}y^+}{\mathrm{d}\bar{u}_{\text{S}}^+} - 1\right)$$
$$= \breve{\nu}_w\kappa_{\text{VK}}e^{-\kappa_{\text{VK}}B}\left[e^{\kappa_{\text{VK}}\bar{u}_{\text{S}}^+} - 1 - \frac{\kappa_{\text{VK}}\bar{u}_{\text{S}}^+}{1!} - \frac{\left(\kappa_{\text{VK}}\bar{u}_{\text{S}}^+\right)^2}{2!}\right]$$
$$\nu_{T_{\text{out}}} = 0.0168\delta_{\text{inc}}^*\bar{u}_{e_{\text{inc}}}\left[1 + 5.5\left(\frac{y}{\delta}\right)^6\right]^{-1} \tag{7}$$

Turbulence Profiles

Then a k–ε formula[12] eddy-viscosity model is used to compute the turbulence Reynolds number by a Newton iteration procedure, and then, when local equilibrium[11] is assumed $(P_k \cong \bar{\rho}_w\varepsilon^*)$, to compute ε^* and k,

$$C_\mu\left(Re_{T_{\text{inc}}}\right)Re_{T_{\text{inc}}}\breve{\nu}_w = \nu_{T_{\text{inc}}}, \qquad \varepsilon^* = \nu_{T_{\text{inc}}}\left(\frac{\mathrm{d}\bar{u}_{\text{inc}}}{\mathrm{d}y}\right)^2$$
$$k = \sqrt{Re_{T_{\text{inc}}}\breve{\nu}_w\varepsilon^*} \tag{8}$$

Then a logarithmic-region turbulence structure (see Ref. 19 and for detailed data compare Refs. 20 and 21), is used to determine normal Reynolds stresses

$$\overline{u'u'} = 2k[1 + \overline{v'v'}/\overline{u'u'} + \overline{w'w'}/\overline{u'u'}]^{-1}$$
$$\overline{u'u'}/\overline{v'v'} = 5.63, \qquad \overline{u'u'}/\overline{w'w'} = 3.15 \tag{9}$$

External Flow Turbulence

When the external flow turbulence intensity T_{u_e} and turbulence length scale ℓ_{T_e} are prescribed and isotropy is assumed $([\overline{u'u'}]_e \cong [\overline{v'v'}]_e \cong [\overline{w'w'}]_e = (T_{u_e}\tilde{u}_e)^2$, and $[\overline{u'v'}]_e = 0)$, a simple matching with the earlier determined profiles is applied using Coles's wake function[17]

$$\overline{u'u'}(y/\delta) \leftarrow |\overline{u'u'} + ([\overline{u'u'}]_e - [\overline{u'u'}]_{\delta^-})\cos[(\pi/2)(1 - y/\delta)]| \tag{10}$$

where $\overline{[.]}_{\delta^-}$ is the previously computed value at the last grid point within the boundary layer and the absolute value is taken to avoid small negative values very near the wall that may appear for high T_{u_e} on fine grids $(y^+ \ll 1)$. Exactly analogous expressions are used for $\overline{v'v'}$ and $\overline{w'w'}$. Then, k, ε^*, Reynolds number $Re_{T_{\text{inc}}}$, $\nu_{T_{\text{inc}}}$, and $\overline{u'v'}$ are recomputed using an iterative procedure. Finally, ε^* is matched by ε_e^*, by an expression analogous to Eq. (10), to conform with ℓ_{T_e}.

Final Profiles

The already obtained incompressible profiles are then transformed to compressible ones using van Driest[13] transformation:

$$\tilde{u} = \frac{\tilde{u}_e}{2\alpha_{\mathrm{VD}}^2}\left\{\sin\left[\alpha_{\mathrm{VD}}\frac{\bar{u}_{\mathrm{inc}}}{\tilde{u}_e} - \operatorname{asin}\left(\frac{\beta_{\mathrm{VD}}}{\sqrt{4\alpha_{\mathrm{VD}}^2+\beta_{\mathrm{VD}}^2}}\right)\right]\right.$$
$$\left.\times\sqrt{4\alpha_{\mathrm{VD}}^2+\beta_{\mathrm{VD}}^2}+\beta_{\mathrm{VD}}\right\} \tag{11}$$

$$\tilde{T} = \tilde{T}_w\left\{1+\frac{\tilde{u}}{\tilde{u}_e}\left[\frac{\tilde{T}_e}{\tilde{T}_w}\left(1+r_f\frac{\gamma-1}{2}\breve{M}_e^2\left(1-\frac{\tilde{u}}{\tilde{u}_e}\right)\right)-1\right]\right\}$$

$$\bar{\rho} = \frac{\bar{p}_e}{\gamma R_g\tilde{T}}, \qquad \bar{\rho}\widetilde{u_i''u_j''} \cong \bar{\rho}\overline{u_i'u_j'} \tag{12}$$

(Reynolds stresses are simply multiplied by $\bar{\rho}[y]$). The adjustment to an external flow turbulence is of major importance, as had already been suggested by Wang et al.[11] in the context of an incompressible flow boundary-layer method with k–ε closure.

Streamwise Decay of Turbulence Intensity

Incoming flow turbulence is prescribed by two parameters, T_{u_∞} and ℓ_{T_∞}, to which it is easy to add anisotropy information, if available. Both these parameters are important because they define the evolution of external flow turbulence, that is, of turbulence intensity at the boundary-layer edge T_{u_e}. If external flow turbulence is isotropic, then the streamwise evolution of turbulence intensity is described by the following equations for k [obtained by taking one-half of the trace of the Reynolds stress transport equations (see Ref. 22)] and ε, written with the asumptions[22] that 1) the mean flow velocity gradients outside the boundary layer are negligible, that is, production $P_k = \frac{1}{2}P_{\ell\ell} \cong 0$, 2) only x-wise gradients exist, and 3) turbulent diffusion is negligible,

$$\frac{\mathrm{D}k_e}{\mathrm{D}t} = \tilde{u}_e\frac{\mathrm{d}k_e}{\mathrm{d}x} \cong -\varepsilon_e \Rightarrow \frac{\mathrm{d}k_e}{\mathrm{d}\left(x\tilde{u}_e^{-1}\right)} \cong -\varepsilon_e$$

$$\frac{\mathrm{D}\varepsilon_e}{\mathrm{D}t} = \tilde{u}_e\frac{\mathrm{d}\varepsilon_e}{\mathrm{d}x} \cong -C_{\varepsilon 2}\frac{\varepsilon_e^2}{k_e} \Rightarrow \frac{\mathrm{d}\varepsilon_e}{\mathrm{d}\left(x\tilde{u}_e^{-1}\right)} \cong -C_{\varepsilon 2}\frac{\varepsilon_e^2}{k_e} \tag{13}$$

which is a system of coupled ordinary differential equations for k_e and ε_e with independent variable the Lagrangian time $t_L = (x-x_1)\tilde{u}_e^{-1}$, that is, the time needed for a fluid particle to go from x_1 to x. It is well known[22] that these equations can be easily integrated analytically provided that $C_{\varepsilon 2}(Re_T) \cong \text{const}$. For the Launder–Sharma[12] dissipation equation used, $C_{\varepsilon 2} = 1.92(1-0.3\mathrm{e}^{-Re_T^{*2}})$, so that $|C_{\varepsilon 2}-1.92| < 1\%$ if $Re_T \geq 1$, that is, almost always except at the final stage of decay. In that case, the following similarity solution is obtained by rewritting Eqs. (13) as

$$\frac{\mathrm{d}k_e}{\mathrm{d}\left(x\tilde{u}_e^{-1}\right)} \cong -\varepsilon_e, \qquad \frac{\mathrm{d}}{\mathrm{d}\left(x\tilde{u}_e^{-1}\right)}\left[\ell\mathrm{n}\left(\frac{k_e^{C_{\varepsilon 2}}}{\varepsilon_e}\right)\right] \cong 0 \qquad (Re_T > 1) \tag{14}$$

$$\eta = \frac{(x-x_1)\varepsilon_1}{\tilde{u}_e k_1} = \frac{\varepsilon_1}{k_1}t_L = \sqrt{\frac{3}{2}}\frac{(x-x_1)}{k_1^{\frac{3}{2}}\varepsilon_1^{-1}}\frac{\sqrt{\frac{2}{3}k_1}}{\tilde{u}_e} = \sqrt{\frac{3}{2}}\frac{(x-x_1)}{\ell_{T_1}}T_{u_1} \tag{15}$$

$$F(\eta) = \frac{1}{(C_{\varepsilon 2}-1)\eta+1}, \qquad k_e(\eta) = k_1[F(\eta)]^{1/(C_{\varepsilon 2}-1)}$$
$$\varepsilon_e(\eta) = \varepsilon_1[F(\eta)]^{C_{\varepsilon 2}/(C_{\varepsilon 2}-1)}$$
$$Re_{T_e}(\eta) = Re_{T_1}[F(\eta)]^{(2-C_{\varepsilon 2})/(C_{\varepsilon 2}-1)}$$
$$T_{u_e}(\eta) = T_{u_1}[F(\eta)]^{1/2(C_{\varepsilon 2}-1)}$$
$$\ell_{T_e}(\eta) = \ell_{T_1}[F(\eta)]^{(-C_{\varepsilon 2}+\frac{3}{2})/(C_{\varepsilon 2}-1)} \tag{16}$$

where η is a nondimensional Lagrangian time, which is the similarity variable of the problem, and k_1, ε_1, Reynolds number Re_{T_1}, T_{u_1}, and ℓ_{T_1} are values at an initial station x_1. Figure 1a shows how turbulence decays in the freestream while its length scale increases. When the expression for the similarity variable η [Eqs. (15)] is used, it is straightforward to reproduce the evolution of external flow turbulence intensity [Eqs. (16)] T_{ue} as a function of $(x-x_1)/\ell_{T_1}$ (Fig. 1b). It is seen that, for $T_{u_1} \cong 1\%$, only 90% $T_{u_1} \cong 0.9\%$ remains at a distance of $\sim 20\ell_{T_1}$ and that this decay is much faster as T_{u_1} increases for example, for $T_{u_1} \cong 5\%$ only 70% T_{u_1} remains after $\sim 20\ell_{T_1}$. It is significant that this evolution is independent of $\tilde{u}_e$ or $\breve{\mu}_e$. This means that if a very small ℓ_{T_1} is applied, then, at a very small distance downstream, almost no turbulence remains, until $\ell_{T_e}(x)$ becomes large enough to slow down axial decay.

Influence of T_{u_∞} and ℓ_{T_∞} on Boundary-Layer Turbulence

Before study is made of the influence of external flow turbulence on shock-wave/boundary-layer interaction, it is necessary to validate the turbulence model ability to predict the influence of T_{u_∞} on boundary-layer velocity and velocity-fluctuation profiles. The experimental data obtained by Raghunathan and McAdam[23] were used for this purpose. These authors[23] measured mean velocity $\tilde{u}_e$ and velocity fluctuations $\widetilde{u''u''}$ for $\breve{M}_e \cong 0.8$ and $Re_\theta \cong 10^4$ zero pressure gradient turbulent boundary layers with varying $T_{u_\delta} = 0.34$–6.3%, where subscripts ∞, e, and δ indicate values corresponding to upstream infinity, outside the boundary layer, and at $y = \delta_{99.5}$ or $y = \delta_{99}$, respectively, so that $\tilde{u}_\delta = 0.995\tilde{u}_e$, $T_{u_\delta} = \sqrt{(\frac{2}{3}k_\delta)}/\tilde{u}_\delta \cong 0.995T_{u_e}$), using a pitot tube and a constant-temperature hot-wire anemometer. The computational domain $L_x \times L_y = 0.5 \times 0.15$ m was meshed

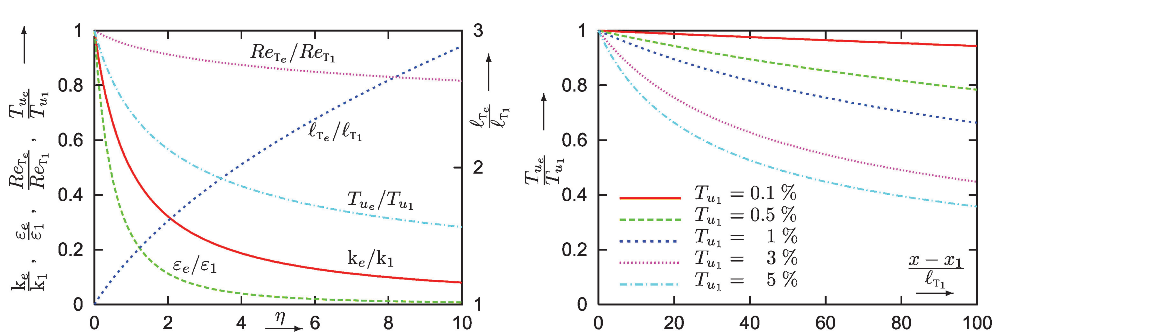

a) b)

Fig. 1 Evolution of decaying freestream turbulence in a uniform mean flow $\tilde{u}_e\vec{e}_x$: a) similarity solution [Eqs. (16)] of relative decay of turbulence parameters $\varepsilon_e, T_{u_e}, \ell_{T_e}$, and Reynolds number Re_{T_e} as a function of the similarity variable (nondimensional Lagrangian time) $\eta = (x-x_1)\,\tilde{u}_e^{-1}/(k_1\varepsilon_1^{-1})$ [Eqs. (15)] and b) turbulence intensity T_{u_e} as a function of the nondimensional axial distance $(x-x_1)/\ell_{T_1}$ for various initial values T_{u_1} [Eqs. (16)].

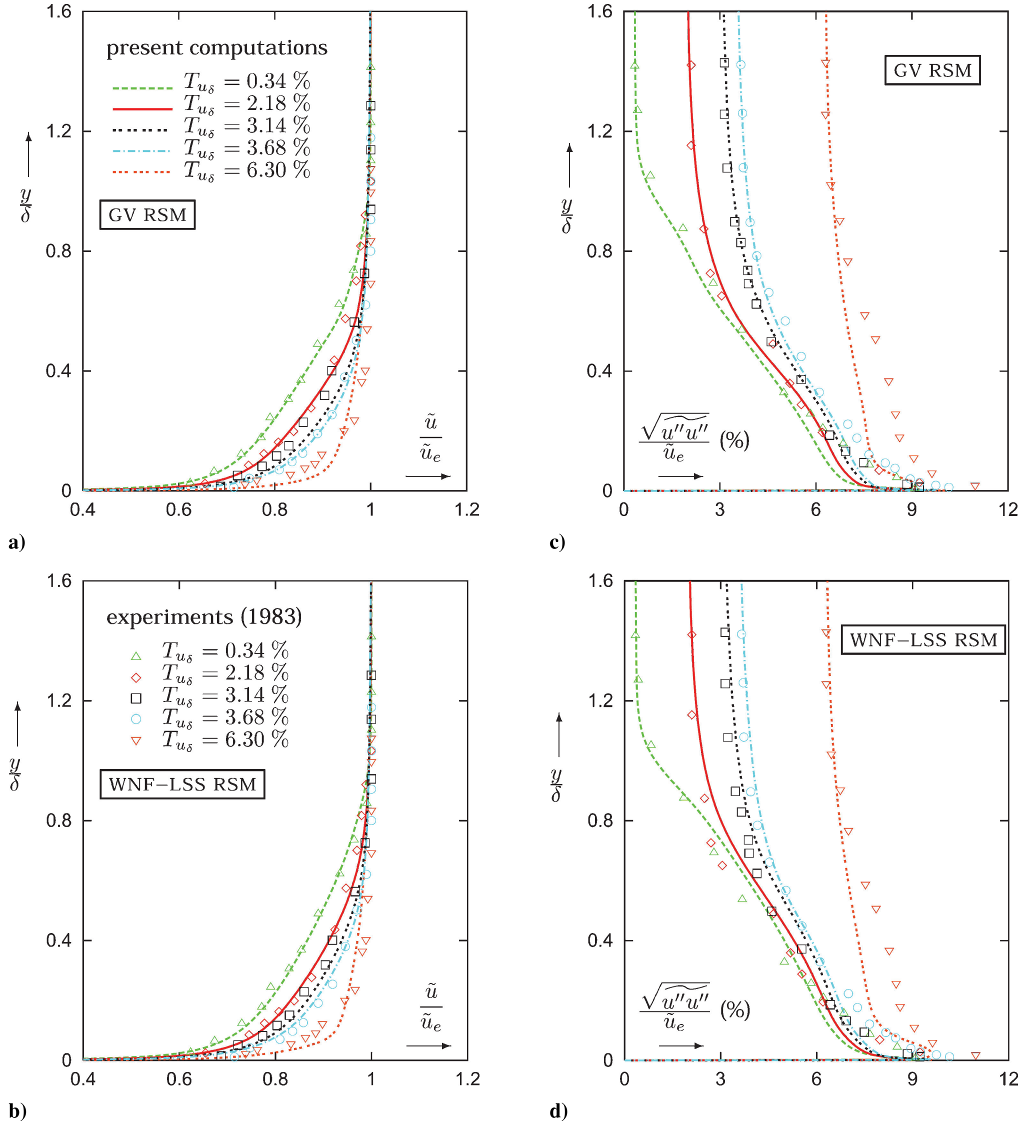

Fig. 2 Influence of turbulence intensity at the boundary-layer edge T_{u_δ} on mean flow velocities (a, b) and on streamwise-velocity fluctuations (c, d), computed on a 401 × 201 grid, using the GV[7] RSM (a, c), and the WNF–LSS[8,9] RSM (b, d), and compared with the experimental measurements of Raghunathan and McAdam[23] for a zero pressure gradient compressible turbulent boundary layer ($\check{M}_e = 0.8$, $Re_\theta \cong 10^4$, and $\ell_{T_e} \cong 1 - 7\delta$).

by a $N_i \times N_j = 401 \times 201$ grid (with $N_{j_s} = 161$ points stretched geometrically near the wall with progression ratio $r_j = 1.05$ and nondimensional distance of the first grid node away from the wall $y_w^+ = 0.5$). At the inflow of the computational domain, a boundary-layer profile was generated with $\Pi_i = 0$, and various δ_i, $T_{u_{e_i}}$, and $\ell_{T_{e_i}}$ were tried until the correct experimental boundary-layer profile (defined by the three parameters $T_{u_\delta} = \sqrt{(\widetilde{u''_\delta u''_\delta})}/\tilde{u}_\delta$, $H = \delta^*/\theta$, and Reynolds number Re_θ) was matched in the interior of the domain. This is in fact an iterative solution of a three-parameter δ_i, $T_{u_{e_i}}$, $\ell_{T_{e_i}}$ optimization problem. In all of the computations, $\ell_{T_e} \cong 2\delta$ in agreement with the experimental estimations[23] ($\ell_{T_e} \cong 1 - 7\delta$).

Comparison of $\tilde{u}/\tilde{u}_e$ and $\sqrt{(\widetilde{u''u''})}/\tilde{u}_e$ for $T_{u_\delta} = \sqrt{(\widetilde{u''_\delta u''_\delta})}/\tilde{u}_\delta =$ 0.34, 2.18, 3.14, 3.68, and 6.3%, using both the GV[7] and WNF–LSS[8,9] RSMs (Fig. 2), shows satisfactory overall agreement. Predictions with both RSMs are quite similar (but not identical). The agreement of mean-velocity profiles with measurements is quite good (Fig. 2) correctly predicting the filling up of the velocity profile near the wall (at constant $Re_\theta \cong 10^4$) as T_{u_δ} increases. With regard to the streamwise normal Reynolds stress $\widetilde{u''u''}$ (Fig. 2), the overall agreement is satisfactory, but when locally $\sqrt{(\widetilde{u''u''})}/\tilde{u}_e > 6\%$, the prediction underestimates the turbulence intensity. This is true $\forall\, T_{u_\delta}$, for example, near the wall for $T_{u_\delta} = 0.34\%$ (Fig. 2). Despite this underestimation, both RSMs predict reasonably well the overall influence of external flow turbulence on the turbulent boundary layer.

Influence of T_{u_∞} on Shock-Wave/ Boundary-Layer Interaction

The method was then used to analyze the effect of external flow turbulence on an $\alpha_c = 24$ deg compression ramp, $M_\infty = 2.85$ and $Re_{\delta_0} = 1.33 \times 10^6$, for which experimental data were obtained by Settles and Dodson,[6] Settles et al.,[24] and Dolling and Murphy[25] at an estimated[26] external flow turbulence intensity $T_{u_\infty} = 1\%$. Computations were run on a 401×201 grid (grid_A in Ref. 9), which is sufficient to obtain reasonably grid-converged results.[9]

Experimental[6,24,25] wall-pressure ($\bar{p}_w/\bar{p}_\infty$) and skin-friction distributions ($C_{f_\infty} = \bar{\tau}_w/[\frac{1}{2}\bar{\rho}_\infty \check{V}_\infty^2]$) vs the curvilinear coordinate s along the ramp are compared with quasi-grid-converged results using both RSM closures for different turbulence intensities $T_{u_\infty} = 0.1$, 0.3, 0.5, 1, 3, and 5% (Fig. 3). It is seen that up to $T_{u_\infty} = 1\%$ the influence is small, whereas for the higher turbulence intensities $T_{u_\infty} = 3\%$ and 5%, the computed separation zone is substantially reduced. On the other hand, the level of C_{f_∞} downstream of the interaction is strongly increased (Fig. 3) with increasing T_{u_∞}. Despite the absence of experimental data for various T_{u_∞} necessary for the validation of the model predictions, results are quite plausible in

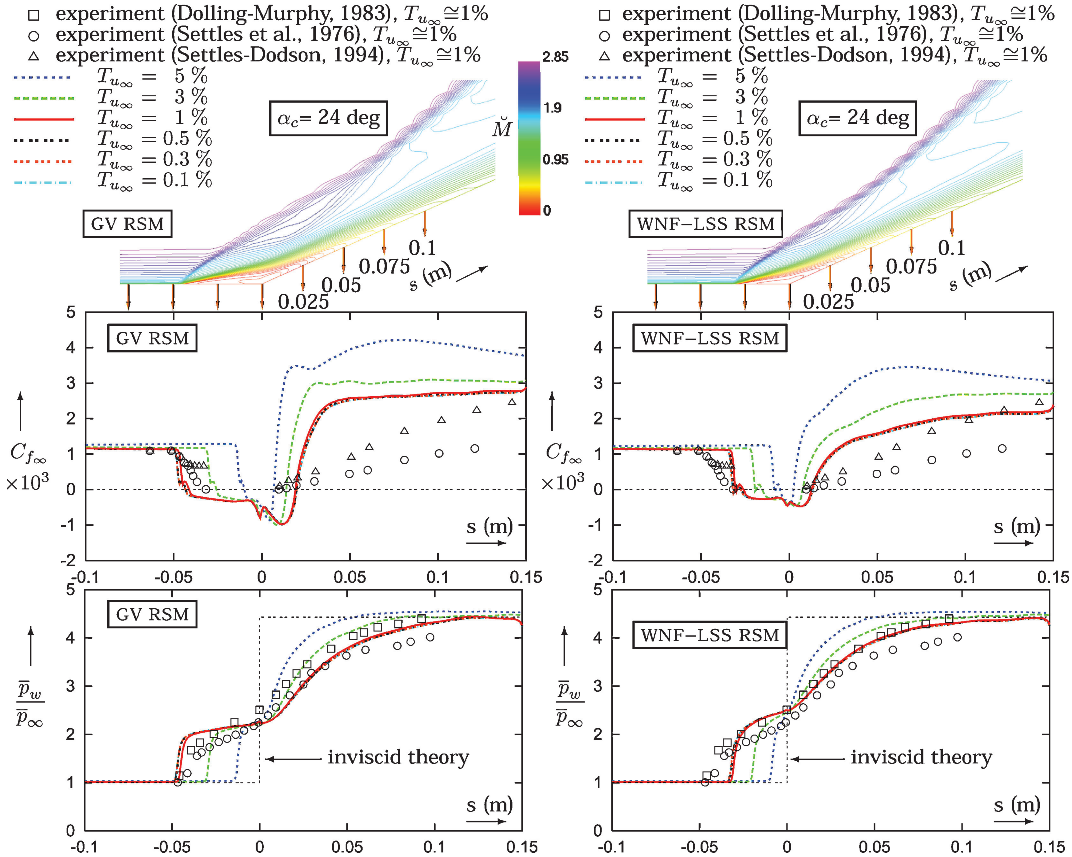

Fig. 3 Influence of incoming flow turbulence intensity T_{u_∞} on s-wise distributions of wall pressure and skin friction for the $\alpha_c = 24$ deg (Refs. 6, 24, and 25) compression-ramp interaction, $M_\infty = 2.85$, $Re_{\delta_0} = 1.33 \times 10^6$, $H_{k_0} = 1.19$, and $\ell_{T_\infty} = 0.025$ m $\cong 1.2\delta_0$, computed on a 401 × 201 grid (grid_A[9]), using GV[7] and WNF–LSS[8,9] RSMs; experiment $T_{u_\infty} \cong 1\%$ and computations $T_{u_\infty} = 0.1$, 0.3, 0.5, 1, 3, and 5%.

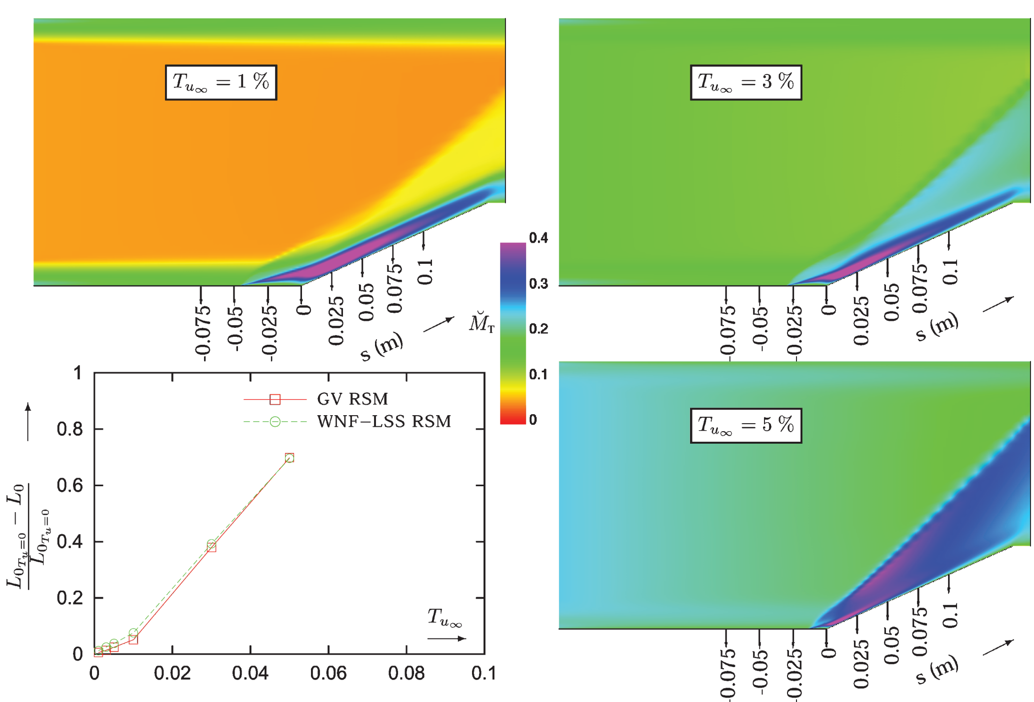

Fig. 4 Turbulence Mach number $\breve{M}_T$ levels, computed on a 401 × 201 grid (grid_A[9]), using GV[7] RSM, for the $\alpha_c = 24$ deg (Refs. 6, 24, and 25) compression ramp interaction, $M_\infty = 2.85$, $Re_{\delta_0} = 1.33 \times 10^6$, $H_{k_0} = 1.19$, and $\ell_{T_\infty} = 0.025$ m $\cong 1.2\delta_0$, for three different levels of incoming flow turbulence intensity $T_{u_\infty} = 1$, 3, and 5%, and relative variations of upstream influence length[1] with respect to the extrapolated value $L_{0_{T_u=0}}$ for $T_{u_\infty} = 0\%$.

indicating a substantial reduction in upstream influence length[1] L_0 and in separated region length. In the present work, the upstream influence length L_0 was measured as the distance from the corner of the point where $\bar{p}_w \cong 1.01\,\bar{p}_\infty$. If the variation of upstream influence length L_0 relative to its $T_{u_\infty} = 0$ value $L_{0_{T_u=0}}$ (obtained by extrapolating the computed results at low T_{u_∞}) is examined, it is seen that the relative effect predicted by both models is very similar (Fig. 4). A reduction of nearly 70% in L_0 is observed for $T_{u_\infty} = 5\%$. The kink on the curve observed for $T_{u_\infty} \cong 1\%$ is also interesting and requires further investigation. Note, considering the $\breve{M}_T = (\sqrt{(2k)})\breve{a}^{-1}$ level plots for various T_{u_∞} (Fig. 4), how for the highest $T_{u_\infty} = 5\%$ an initial decay of external flow turbulence is visible, in accordance with the earlier analysis (Fig. 1b), which predicts a faster decay for higher T_{u_1} at fixed ℓ_{T_1}.

Conclusions

Two previously validated near-wall WNF RSMs were used to investigate the influence of inflow conditions on supersonic ($M_{\mathrm{SW}} = 2.85$) oblique-shock-wave/turbulent-boundary-layer interactions with large separation, and the following conclusions were obtained:

1) A simple semi-analytic procedure for generating inflow (and initial) profiles for mean flow and turbulence variables that includes arbitrarily prescribed external flow turbulence intensity and length scale, wall temperature, and boundary-layer shape factor was described in detail and validated.

2) The choice of the external flow turbulence length scale at inflow ℓ_{T_∞} should not be made arbitrarily because it defines the streamwise rate of decay of turbulence intensity T_{u_e} and, as a consequence, the turbulence intensity at the beginning of the interaction; this choice has an increasing influence on decay as T_{u_∞} increases.

3) Turbulence intensity of the incoming flow has a small (but not negligible) influence on upsteam interaction length at low T_{u_∞} ($\sim$7% difference between $T_{u_\infty} = 0$ and $T_{u_\infty} = 1\%$) and a much stronger one for higher T_{u_∞} ($\sim$65% difference between $T_{u_\infty} = 5\%$ and $T_{u_\infty} = 0\%$); increasing T_{u_∞} diminishes upstream interaction length, retards separation, and accelerates reattachment.

Acknowledgments

This work was partly supported by Project T0216-0219 of the Supersonic Research Initiative of the French Ministry of Research, coordinated by A. Lerat. The computations were run at the Institut pour le Développement des Ressources en Informatique Scientifique. The authors are listed alphabetically.

References

[1] Délery, J. M., "Shock-Wave/Turbulent-Boundary-Layer Interaction and its Control," *Progress in Aerospace Science*, Vol. 22, 1985, pp. 205–280.

[2] Dolling, D. S., "Fifty Years of Shock-Wave/Boundary-Layer Interaction Research: What Next?" *AIAA Journal*, Vol. 39, No. 8, 2001, pp. 1517–1531.

[3] Raghunathan, S., and McAdam, R. J. W., "Freestream Turbulence and Transonic Flow over a 'Bump' Model," *AIAA Journal*, Vol. 21, No. 3, 1983, pp. 467–469.

[4] Raghunathan, S., and McAdam, R. J. W., "Relative Effects of Reynolds-Number and Freestream Turbulence in Transonic Flow," *AIAA Journal*, Vol. 23, No. 4, 1985, pp. 546–550.

[5] Hamed, A., and Shang, J. S., "Survey of Validation Data Base for Shock-wave Boundary-Layer Interactions in Supersonic Inlets," *Journal of Propulsion and Power*, Vol. 7, 1991, pp. 617–625.

[6] Settles, G. S., and Dodson, L. J., "Supersonic and Hypersonic Shock/Boundary-Layer Interaction Database," *AIAA Journal*, Vol. 32, No. 7, 1994, pp. 1377–1383.

[7] Gerolymos, G. A., and Vallet, I., "Wall-Normal-Free Near-Wall Reynolds-Stress Closure for Three-Dimensional Compressible Separated Flows," *AIAA Journal*, Vol. 39, No. 10, 2001, pp. 1833–1842.

[8] Gerolymos, G. A., Sauret, E., and Vallet, I., "Contribution to the Single-Point-Closure Reynolds-Stress Modelling of Inhomogeneous Flow," *Theoretical and Computational Fluid Dynamics* (to be published).

[9] Gerolymos, G. A., Sauret, E., and Vallet, I., "Oblique-Shock-Wave/Boundary-Layer Interaction Using Near-Wall Reynolds Stress Models," *AIAA Journal*, Vol. 42, No. 6, 2004, pp. 1089–1100; also AIAA Paper 2003-3466, June 2003.

[10] Rizzetta, D. P., "Evaluation of Explicit Algebraic Reynolds-Stress Models for Separated Supersonic Flows," *AIAA Journal*, Vol. 36, No. 1, 1998, pp. 24–30.

[11] Wang, J. H., Jen, H. F., and Hartel, E. O., "Airfoil Heat Transfer Calculation Using a Low-Reynolds-Number Version of a 2-Equation Turbulence Model," *Journal of Engineering for Gas Turbines and Power*, Vol. 107, 1985, pp. 60–67.

[12] Launder, B. E., and Sharma, B. I., "Application of the Energy Dissipation Model of Turbulence to the Calculation of Flows near a Spinning Disk," *Letters in Heat and Mass Transfer*, Vol. 1, 1974, pp. 131–138.

[13] Van Driest, E. R., "Turbulent Boundary-Layer in Compressible Fluids," *Journal of the Aeronautical Sciences*, Vol. 18, No. 3, 1951, pp. 145–160, 216.

[14] Maise, G., and McDonald, H., "Mixing Length and Kinematic Eddy Viscosity in a Compressible Boundary Layer," *AIAA Journal*, Vol. 6, No. 1, 1968, pp. 73–80.

[15] Smits, A. J., and Dussauge, J. P., *Turbulent Shear Layers in Supersonic Flow*, AIP Press, Woodbury, NY, 1996, pp. 115–131.

[16] Spalding, D. B., "A Single Formula for the Law-of-the-Wall," *Journal of Applied Mechanics*, Vol. 28, 1961, pp. 455–458.

[17] Coles, D., "The Law of the Wake in a Turbulent Boundary Layer," *Journal of Fluid Mechanics*, Vol. 1, 1956, pp. 191–226.

[18] Clauser, F. H., "The Turbulent Boundary-Layer," *Advances in Applied Mechanics*, Vol. 4, 1956, pp. 1–51.

[19] Laufer, J., "Some Recent Measurements in a 2-D Turbulent Channel," *Journal of the Aeronautical Sciences*, Vol. 17, 1950, pp. 277–287.

[20] Laufer, J., "Investigation of Turbulent Flow in a Two-Dimensional Channel," NACA TN 2123, July 1950.

[21] Laufer, J., "Investigation of Turbulent Flow in a Two-Dimensional Channel," NACA Rept. 1053, 1951.

[22] Wilcox, D. C., *Turbulence Modelling for CFD*, 2nd ed., DCW Industries, La Cañada, CA, 1998, pp. 150–172.

[23] Raghunathan, S., and McAdam, R. J. W., "Freestream Turbulence Effects on Attached Subsonic Turbulent Boundary-Layers," *AIAA Journal*, Vol. 21, No. 4, 1983, pp. 503–508.

[24] Settles, G. S., Vas, I. E., and Bogdonoff, S. M., "Details of a Shock-Separated Turbulent/Boundary-Layer at a Compression Corner," *AIAA Journal*, Vol. 14, No. 12, 1976, pp. 1709–1715.

[25] Dolling, D. S., and Murphy, M. T., "Unsteadiness of the Separation Shock-Wave Structure in a Supersonic Compression Ramp Flowfield," *AIAA Journal*, Vol. 21, No. 12, 1983, pp. 1628–1634.

[26] Fernholz, H. H., Finley, P. J., Dussauge, J. P., and Smits, A. J., "A Survey of Measurements and Measuring Techniques in Rapidly Distorted Compressible Turbulent Boundary Layers," AGARDograph 315, AGARD, May 1989.

R. So
Associate Editor

Color reproductions courtesy of Université Pierre-et-Marie Curie.